Heliyon 10 (2024) e35588

Contents lists available at ScienceDirect

Heliyon

journal homepage: www.cell.com/heliyon

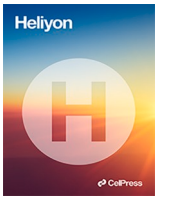

Research article

Synthesis and synergistic antibacterial efficiency of chitosan-copper oxide nanocomposites

Jüri Laanoja [a,b], Mariliis Sihtmäe [a], Svetlana Vihodceva [c], Mairis Iesalnieks [c], Maarja Otsus [a], Imbi Kurvet [a], Anne Kahru [a,d], Kaja Kasemets [a,*]

[a] Laboratory of Environmental Toxicology, National Institute of Chemical Physics and Biophysics, Akadeemia tee 23, 12618 Tallinn, Estonia
[b] Department of Chemistry and Biotechnology, School of Science, Tallinn University of Technology, Ehitajate tee 5, 19086 Tallinn, Estonia
[c] Institute of Materials and Surface Engineering, Faculty of Natural Sciences and Technology, Riga Technical University, Paula Valdena 3/7, LV-1048 Riga, Latvia
[d] Estonian Academy of Sciences, Kohtu 6, 10130 Tallinn, Estonia

ARTICLE INFO

Keywords:
Antimicrobial nanocomposites
Chitosan
Particle-cell interactions
Copper bioavailability
Synergy

ABSTRACT

Copper and chitosan are used for biomedical applications due to their antimicrobial properties. In this study, a facile method for the synthesis of chitosan-copper oxide nanocomposites (nCuO-CSs) was modified, yielding stable colloidal nCuO-CSs suspensions. Using this method, nCuO-CSs with different copper-to-chitosan (50–190 kDa) weight ratios (1:0.3, 1:1, 1:3) were synthesized, their physicochemical properties characterized, and antibacterial efficacy assessed against Gram-negative *Escherichia coli* and *Pseudomonas aeruginosa*, and Gram-positive *Staphylococcus aureus*. The nCuO-CSs with a primary size of ~10 nm and a ζ-potential of >+40 mV proved efficient antibacterials, acting at concentrations around 1 mg Cu/L. Notably, against Gram-negative bacteria, this inhibitory effect was already evident after a 1-h exposure and surpassed that of copper ions, implying to a synergistic effect of chitosan and nano-CuO. Indeed, using flow cytometry and confocal laser scanning microscopy, we showed that chitosan promoted interaction between the nCuO-CSs and bacterial cells, facilitating the shedding of copper ions in the close vicinity of the cell surface. The synergy between copper and chitosan makes these nanomaterials promising for biomedical applications (e.g., wound dressings).

1. Introduction

Antimicrobial resistance (AMR) is among the most distressing and urgent healthcare problems worldwide [1]. Global access to antibiotics and the means to monitor antibiotic consumption vary greatly, leading to their misuse [2]. What is more, AMR is often the culprit behind hospital-acquired infections. In Europe, roughly a third of the 8.9 million yearly hospital-acquired infections in 2016 and 2017 were linked to antibiotic-resistant bacteria [3]. According to an extensive systematic analysis [4], *Escherichia coli*, *Staphylococcus aureus*, *Klebsiella pneumoniae*, *Streptococcus pneumoniae*, *Acinetobacter baumannii*, and *Pseudomonas aeruginosa* were estimated to have been responsible for >70 % of the deaths attributable to (1.27 million) and associated with (4.95 million) AMR in 2019. Efficient antimicrobials are needed to combat this persistent threat.

Nanotechnology holds great promise for the development of novel and effective antimicrobials, but also for the remediation of

* Corresponding author.
E-mail address: kaja.kasemets@kbfi.ee (K. Kasemets).

https://doi.org/10.1016/j.heliyon.2024.e35588
Received 9 May 2024; Received in revised form 12 July 2024; Accepted 31 July 2024
Available online 2 August 2024
2405-8440/© 2024 The Authors. Published by Elsevier Ltd. This is an open access article under the CC BY-NC-ND license (http://creativecommons.org/licenses/by-nc-nd/4.0/).

water and air pollution [5–9]. Due to their small size and proportionally large specific surface area, nanomaterials exhibit distinct properties compared to bulk materials of similar composition [10,11]. While bacteria possess various defense mechanisms against toxic agents, metallic nanoparticles (NPs) act against bacteria via multiple means and are thus believed to be less likely to cause the development of AMR [12–14]. This topic has not been studied extensively, and early reports are divisive [15–17]. Still, certain metallic nanoparticles, e.g., Ag, CuO, and ZnO, are already used for biomedical applications, primarily due to their antimicrobial properties [18]. Notably, various forms of silver and copper have been used for antimicrobial purposes for centuries. Furthermore, as an essential microelement, copper is needed in all the stages of wound healing [19,20]. The stability and/or functionality of NPs is often improved by covering them with various capping agents, e.g., polyvinylpyrrolidone, polyethylene glycol, bovine serum albumin, or chitosan [21]. Alternatively, nanoparticles can be embedded in the matrix of a polymer to form nanocomposites – mixtures of two or more phase-separated materials with at least one being at the nanoscale (at least one dimension sized at 1–100 nm) [22].

Chitosan is a biodegradable polysaccharide comprised of randomly distributed D-glucosamine and *N*-acetyl-D-glucosamine residues linked via β-1,4-glycosidic bonds. On a commercial scale, chitosan is mainly produced by the deacetylation of chitin. The latter is usually extracted from crustacean shell waste, a major food industry byproduct. Chitosan's molecular weight (MW) and degree of deacetylation (DDA) vary based on the conditions (temperature, duration, etc.) of the preceding chemical treatment (a thorough overview of the production process is provided elsewhere [23]). Hence, low-, medium-, and high molecular weight chitosan are distinguished (the generally referenced values are 50–190, 190–310, and 310–375 kDa, respectively, but literature data are inconsistent [24]). Thanks to its biocompatible, antimicrobial, and immune-modulating properties, chitosan is used in wound treatment (hydrogels, bandages, etc.) [24–27]. The antimicrobial efficacy and wound healing potential of copper in combination with chitosan is an intriguing research topic that has not been studied widely.

In this study, a straightforward method for the synthesis of chitosan-copper oxide nanocomposites (nCuO-CSs) was developed for potential application in wound dressings. The precursor, copper(II) acetate, was precipitated by sodium hydroxide in the presence of chitosan. Nanocomposites with three copper to chitosan mass ratios (1:0.3, 1:1, 1:3) were prepared. The nCuO-CSs physicochemical characteristics were determined by dynamic light scattering, electrophoretic light scattering, X-ray diffraction (XRD), X-ray photoelectron spectroscopy (XPS), Fourier-transform infrared spectroscopy (FTIR), transmission electron microscopy (TEM), and field emission scanning electron microscopy coupled with energy-dispersive X-ray spectroscopy (FESEM-EDS). In addition, the antibacterial efficacy of the nCuO-CSs was assessed against four clinically relevant bacterial strains: Gram-negative *E. coli* (MG1655 and ATCC 25922) and *P. aeruginosa* ATCC 27853, and Gram-positive *S. aureus* ATCC 6538. Interactions between nCuO-CSs and bacterial cells were analyzed by flow cytometry and confocal laser scanning microscopy.

2. Materials and methods

2.1. Materials

Low molecular weight chitosan (50–190 kDa, 75–85 % deacetylated), copper(II) acetate (≥98 %), sodium chloride (NaCl, ≥99 %), sodium phosphate monobasic (dihydrate, ≥99 %), sodium phosphate dibasic (anhydrous, ≥95 %), hydrogen peroxide solution (H_2O_2, 30 %), ampicillin sodium salt, tetracycline (≥98 %), propidium iodide (PI, >95 %), CuO nanopowder (<50 nm, product number 544868), and 3-(N-morpholino)propanesulfonic acid (MOPS, ≥99 %) were purchased from Sigma-Aldrich; agar, tryptone, yeast extract, and acid hydrolyzed casein (casamino acids) from Neogen (Heywood, UK); sodium hydroxide (NaOH, ≥98 %) from Chemapol Group, a.s. (Prague, Czech Republic); 2′,7′-dichlorodihydrofluorescein diacetate (≥95 %) from Cayman Chemicals (Ann Arbor, MI, USA); absolute ethanol from Berner Oy (Helsinki, Finland); MycoLight™ Green JJ98 (≥95 %) from AAT Bioquest, Inc. (Sunnyvale, CA, USA); glucose from Armila (Vilnius, Lithuania); SYTO 9 from Thermo Fisher Scientific (Waltham, MA, USA); and nitric acid (HNO_3, ≥65 %) from Honeywell (Seelze, Germany). Ultrapure water (18.2 MΩ cm @ 25 °C, TOC <5 ppb; henceforth DI water) was prepared on site (Milli-Q Direct-Q 3 UV Water Purification System, Merck KGaA, Darmstadt, Germany).

2.2. Synthesis of chitosan-copper oxide nanocomposites

A 1 % (w/v) chitosan (CS; 50–190 kDa) solution was prepared in 1 % (v/v) acetic acid with continuous stirring for at least 24 h at room temperature. Three dilutions of CS in DI water (0.033, 0.11, and 0.22 %) were prepared shortly before the synthesis and filtered using either a 0.45 μm (0.033 and 0.11 % CS) or a 1.2 μm (0.22 % CS) syringe filter (Sarstedt, Nümbrecht, Germany). A copper(II) acetate solution (1100 mg Cu/L) was prepared in deionized (DI) water and filtered (0.2 μm). Chitosan-copper oxide nanocomposites were synthesized via a modified method described by Gvozdenko et al. [28]. Briefly, a 28.5 mL reaction mixture (550 mg Cu/L) of copper(II) acetate and chitosan was prepared with varying mass ratios of copper to chitosan (Cu:CS; 1:0.3, 1:1, 1:2) and heated to 80 °C on a magnetic stirrer with temperature control (C-MAG HS 7 Package, IKA, Staufen, Germany). Based on Cu:CS mass ratio, approximately 0.55, 0.8 or 1.1 mL of 1M NaOH was added dropwise, after which the temperature was kept at 80 °C for an additional 10 min. Subsequently, the solution was cooled to room temperature in a water bath, and the resulting volume measured. DI water was added to samples with 1:0.3 and 1:1 Cu:CS ratios to increase the volume to 30 mL. To the sample with a 1:2 Cu:CS ratio, an aliquot of 0.3 % CS solution (pH 7) was added to raise the Cu:CS ratio to 1:3 and the volume to 30 mL. The samples were then sonicated (Branson Digital Sonifier 450, Branson Ultrasonics Corporation, Danbury, CT, USA) for 30 s at 10 % amplitude (40 W) and finally dialyzed (cut-off 12 000 kDa, Viskase, Chicago, IL, USA) against 2 L of DI water for a total of 48 h (the DI water was changed after 24 h). A simplified schematic representation of the synthesis process is displayed in Fig. S1.

2.3. Physicochemical characterization of chitosan-copper oxide nanocomposites

Average hydrodynamic size (dh), zeta (ζ) potential and polydispersity index (PDI) of the synthesized nCuO-CSs in DI water at 40 mg Cu/L were measured by Zetasizer Nano ZS (Malvern Panalytical, Worcestershire, UK) using DTS1061 folded capillary cuvettes (Malvern Panalytical). The reported dh, ζ-potential, and PDI values are measurement averages of three separate syntheses. Transmission electron microscopy (TEM) analysis was commissioned from the University of Tartu (Estonia), and the primary size of the nCuO-CSs determined from the corresponding TEM images with ImageJ 1.54d software. Lyophilized samples were used for X-ray diffraction (XRD), X-ray photoelectron spectroscopy (XPS), Fourier-transform infrared spectroscopy (FTIR), field emission scanning electron microscopy (FESEM) and energy-dispersive X-ray spectroscopy (EDS) analyses.

Crystalline phases of the nCuO-CSs were analyzed by XRD (Rigaku MiniFlex, Tokyo, Japan) with Cu Kα (λ 1.540593 Å) radiation in the scan range 5–90° and 2°/min scanning speed. XPS spectra were generated using an Escalab Xi + spectrometer (Thermo Fisher Scientific, Waltham, MA, USA) with a 500 μm spot size and an aluminium K-Alpha X-ray source, and data analysis was performed with the accompanying Avantage 5.9925 software and an advantageous carbon peak at 284.8 eV used as a calibration point. Infrared spectra of KBr pellets containing the sample (0.1 wt%) were recorded in the 4000–400 cm^{-1} range with 60 scans using the IRPrestige-21 FTIR spectrometer (Shimadzu, Tokyo, Japan). The morphology and chemical composition of the nCuO-CSs was characterized by FESEM (Lyra, FEI NanoSEM 650, Eindhoven, Netherlands) coupled with EDS (TEAM™ Integrated EDS with Apollo X SDD, EDAX, Pleasanton, CA, USA).

2.4. Quantification of dissolved copper ions

The amount of Cu ions leached from the nCuO-CSs in DI water was determined at 1 and 10 mg Cu/L. Briefly, 4 mL of each nCuO-CSs sample was pipetted to a 6-well microplate well (Corning Incorporated, Corning, NY, USA) and incubated for 1 or 24 h (30 °C in the dark). After incubation, 3.5 mL of the sample was transferred to a centrifugal filter tube (Amicon Ultra-4, 3000 NMWL, Millipore, Carrigtwohill, Ireland) and centrifuged (Sigma 3-16 PK, Sigma Laborzentrifugen GmbH, Osterode, Germany) for 40 min at 6225 g, 30 °C. Concentrated HNO_3 was added to the filtrate to a total volume of 5 %, the sample vortexed thoroughly, and the Cu content measured by atomic absorption spectroscopy (AAS, contrAA 800, Analytic Jena, Jena, Germany).

2.5. Determination of minimum biocidal concentration

The antibacterial efficacy of the synthesized nCuO-CSs against clinically relevant Gram-negative bacteria *E. coli* MG1655 (*E. coli* Genetic Stock Center, Yale University, New Haven, CT, USA), *E. coli* ATCC 25922 (American Type Culture Collection, Manassas, VA, USA), *P. aeruginosa* ATCC 27853 and Gram-positive bacteria *S. aureus* ATCC 6538 was determined by the cell viability test – 'spot test' – in DI water [29]. In short, bacteria from an exponentially growing culture ($OD_{600} = 0.6$) in Luria-Bertani medium (LB, 10 g/L tryptone, 5 g/L yeast extract, 5 g/L NaCl) were washed twice by centrifugation (7 min, 5094 g; Sigma 3-16 PK, Sigma Laborzentrifugen GmbH, Osterode, Germany) and resuspended in DI water. Then the bacterial suspension was diluted to $OD_{600} = 0.1$, and aliquots of 100 μL were mixed with an equal volume of nCuO-CSs (at progressively lower concentrations) in DI water in 96-well microplate wells (Corning Incorporated, Corning, NY, USA). The plates were incubated in the dark for up to 24 h at 30 °C. 3 μL from each well were pipetted on LB agar (15 g/L agar) plates at 1, 4 and 24 h. The agar plates were incubated at 30 °C for 24 h, after which the minimum biocidal concentration (MBC) was visually determined to be the lowest concentration of nCuO-CSs that prevented the formation of bacterial colonies. DI water was used as a negative- and copper(II) acetate as an ionic control. Chitosan (50–190 kDa) and commercial CuO NPs (Sigma-Aldrich, St. Louis, MO, USA) were used for comparison. Each test was repeated at least thrice, always with duplicate samples.

2.6. Quantification of bioavailable copper fraction

The bioavailable copper in the nCuO-CSs suspensions was quantified using Cu- and Ag-induced recombinant bioluminescent sensor bacteria *E. coli* MC1061(pSLcueR/pDNPcopAlux), as described by Heinlaan et al., 2008 [30]. In parallel, control bacteria *E. coli* MC1061(pDNlux), which constitutively express luminescence genes, were tested to account for the nanosuspension's turbidity and toxicity.

The bacteria were cultivated in accordance to section 2.5. with few modifications: (i) for both bacteria, the LB medium was supplemented with 10 mg/L tetracycline; (ii) 100 mg/L ampicillin was added only for the sensor bacteria; (iii) after the washing steps, the bacteria were resuspended in an induction medium – a 40 mM 3-(N-morpholino)propanesulfonic acid (MOPS) solution in DI water (pH 6.5) with 0.1 % (w/v) acid hydrolyzed casein and 0.1 % (w/v) glucose.

For the bioavailability assay, 100 μL of the nCuO-CSs (0.002–1 mg Cu/L) or $CuSO_4$ (0.0002–10 mg Cu/L) dilutions in DI water were added to the wells of white 96-well polypropylene microplates (Greiner Bio-One, Frickenhausen, Germany), DI water was added to separate wells for background luminescence determination. Then, 100 μL of bacterial (either sensor or control) suspension was added to the wells. The microplates were incubated at 30 °C in the dark for up to 2 h, the optimal time for the sensor bacteria induction. Hence, the bioavailable copper was quantified after 1 and 2 h exposure to the tested chemicals, unlike the viability test (section 2.5.). Bacterial bioluminescence was measured using an Orion II Plate Luminometer (Berthold Detection Systems, Pforzheim, Germany). The fold induction (FI) in bioluminescence, caused by bioavailable/intracellular copper compared to the background values (i.e., bioluminescence of sensor bacteria in DI water), was calculated. The bioavailable copper from the tested nCuO-CSs was quantified based on

a calibration curve of $CuSO_4$ (X–Y plot of Cu concentration versus FI), considering $CuSO_4$ 100 % bioavailable. The experiments were conducted three to four times, each with duplicate samples.

2.7. Measurement of abiotic and biotic reactive oxygen species

2′,7′-dichlorodihydrofluorescein diacetate ($DCFH_2$-DA) assays were performed to evaluate the nCuO-CSs potential to cause the formation of reactive oxygen species (ROS). The tests in abiotic (i.e., without bacteria) conditions were performed as described by Aruoja et al. [31], and the capacity of the nCuO-CSs to induce intracellular (biotic) ROS generation was determined as detailed by Käosaar et al. [32]. A full outline for these analyses is included in section S1.

2.8. Flow cytometry

Flow cytometry was used to assess the interaction between bacterial cells and the synthesized nCuO-CSs, as described by Feng et al. [33]. The bacterial suspensions were prepared as detailed in section 2.5. and the bacteria exposed to nCuO-CSs at two concentrations (0.25 and 1 mg Cu/L for the Gram-negative bacteria, 1 and 15 mg Cu/L for *S. aureus*). For that, 250 μL of bacterial suspension was added to an equivalent volume of nCuO-CSs in DI water and incubated for 1 h at 30 °C in the dark. Afterwards, the bacteria were stained (15 min, room temperature) with 0.5 μL of MycoLight™ Green JJ98. Before measurements, the samples were diluted thrice with DI water, and two 500 μL aliquots from each sample were analyzed on a BD Accuri™ C6 flow cytometer (BD Biosciences, Ann Arbor, MI, USA). The resulting data was processed by BD Accuri™ C6 software. 20 000 cells were analyzed from each sample, and interactions between bacteria and nCuO-CSs attributed to the increase in side scattered light intensity compared to the (unexposed) control cells. Each test was performed twice.

2.9. Confocal laser scanning microscopy

Confocal laser scanning microscopy was used to visualize bacterial interactions with the synthesized nCuO-CSs. Bacterial cultures were prepared and processed as described in Section 2.5. Following centrifugation (1 min, 9300 g), the cells were resuspended in DI water to an $OD_{600} = 0.5$ and then exposed to nCuO-CSs at a concentration of 1 mg Cu/L and chitosan at 1 and 3 mg/L for 1 h at 30 °C. In the case of *S. aureus*, the nCuO-CSs were also studied at 10 mg Cu/L and chitosan at 10 and 30 mg/L. After the incubation, the cell suspension was stained with SYTO 9 to a final concentration of 5 μM for 10 min in the dark. Subsequently, 20 μL of the stained cell suspension was spread on a microscopy slide, dried at 37 °C for 15 min, mounted in Mowiol (Sigma-Aldrich, Darmstadt, Germany) and covered with a cover glass. The samples were visualized with Zeiss LSM800 CLSM (Zeiss, Jena, Germany) using a 488 nm laser and 505–550 nm emission filter to acquire a SYTO 9 signal. Images were processed using ZEN software.

In addition, potential membrane damage caused by the nCuO-CSs was assessed. The cells were stained with propidium iodide (81 845; Sigma-Aldrich, Steinheim, Germany), which penetrates only cells with damaged membranes, and SYTO 9 (S34854; Thermo Fisher Scientific, Waltham, MA, USA), which can enter both damaged and intact cells. The overview of this analysis is included in section S2.

2.10. Statistical analysis

Due to a moderate number of replicate experiments (4–6), the nonparametric Kruskal-Wallis test was performed to establish any statistically significant differences in the MBC values of the three nCuO-CSs for all the tested bacteria. If the null hypothesis was rejected, the Bonferroni corrected Dunn's test was used for *Post hoc* pairwise comparison. For both tests, the significance level was set at 0.05. The IBM SPSS Statistics (version 29.0) software suite was used for statistical analysis.

3. Results and discussion

3.1. Synthesis and physicochemical characterization of chitosan-copper oxide nanocomposites

Gvozdenko et al. [28] analyzed CuO NPs obtained from different precursor salts: copper(II) acetate, copper(II) chloride, and copper (II) sulfate. Based on XRD analysis, they achieved monophase CuO NPs only when copper(II) acetate was used. Hence, in this study, copper(II) acetate was chosen as the precursor salt for nCuO-CSs synthesis. Generally, NaOH has been used for the synthesis of CuO nanoparticles via precipitation [28,34,35]. However, our preliminary experiments showed that nCuO-CSs formed via precipitation were prone to aggregation and, between batches, highly variable in hydrodynamic size (dh) – the average dh of the four initial batches was ~840 nm with a coefficient of variation of ~50 % (data not shown; the used Cu to chitosan mass ratio was 1:1). It must be noted that Gvozdenko et al. [28] used gelatin, and not chitosan, as a stabilizer. A possible reason for aggregation might originate from the fact that chitosan (pKa 6.3–6.5) is insoluble in alkaline media [24,36]. To overcome aggregation, the volume of NaOH required for the visible precipitation of CuO was first determined. Accordingly, a lower amount of NaOH (i.e., that did not cause the precipitation of CuO; as specified in section 2.2.) was used in the following syntheses. Yet, stopping the reaction 'prematurely' may have resulted in the presence of both CuO and Cu_2O species in the chitosan matrix, as shown by the XPS analysis (section 3.3.), or Cu(I) defects in the CuO crystal lattice.

Three batches of nCuO-CSs (Fig. 1a) were synthesized in three Cu:CS mass ratios – 1:0.3, 1:1, 1:3 – which are henceforth designated

as nCuO-CS_0.3, nCuO-CS_1, and nCuO-CS_3, respectively. Based on TEM analysis, the nCuO-CSs were agglomerates of up to 100 nm (Fig. 1c), composed of smaller particles with a primary size of 8.1 ± 1.4 nm (Fig. 1b–d).

Based on three separate syntheses, the average hydrodynamic sizes (dh) of the nCuO-CSs in DI water were 88 ± 5.7 nm, 124 ± 20

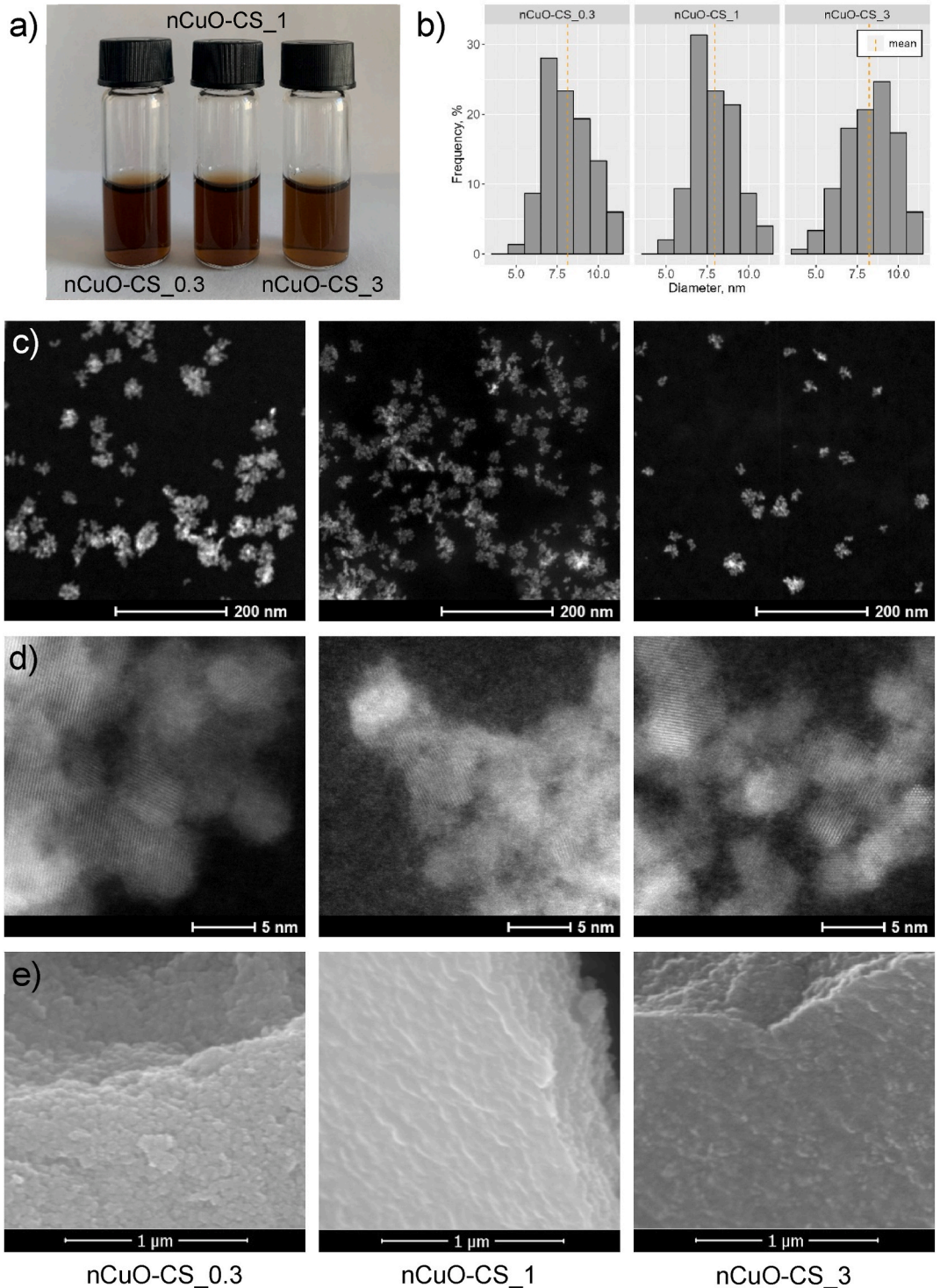

Fig. 1. Characterization of chitosan-copper oxide nanocomposites (nCuO-CSs). (a) The nCuO-CSs suspensions after dialysis. (b) The primary size distribution of nCuO-CSs. (c), (d) TEM and (e) SEM images of lyophilized nCuO-CSs. nCuO-CS_0.3, nCuO-CS_1, and nCuO-CS_3 designate different Cu:chitosan mass ratios (1:0.3, 1:1, and 1:3, respectively).

nm, and 182 ± 1.9 nm (Table 1) for nCuO-CS_0.3, nCuO-CS_1, and nCuO-CS_3, respectively. The polydispersity index (PDI) was slightly higher for nCuO-CSs with greater chitosan content, with values < 0.35 (PDI values of 0.1–0.4 are considered to be moderately polydisperse [37]). At the same time, ζ-potential was >+40 mV for all synthesized nCuO-CSs (colloidal dispersions with an absolute ζ-potential value of >30 mV are generally regarded stable; nevertheless, deviations are not uncommon [37]). The dh, ζ-potential, and PDI of the nCuO-CSs used in ensuing experiments were measured periodically (Table S1) and did not change noticeably. Likewise, the nCuO-CSs showed no visible signs of precipitation after 6 months of storage at 4 °C in the dark.

Based on FESEM images (Fig. 1e–S2), the lyophilized nCuO-CSs resemble sheet-like structures. Table S2 shows the elemental composition of the nCuO-CSs as determined by EDS compared to the surface characterization by XPS. In addition to verifying the presence of elements occurring naturally in chitosan (carbon, oxygen, nitrogen) and copper, the lack of contamination by other elements was established. The XRD analysis indicates that the crystalline phase of nCuO-CSs matches the CuO mineral tenorite (ICDD 99-000-3666; Fig. 2a).

3.2. FTIR analysis

Infrared spectroscopy was performed to elucidate the possible interaction between chitosan and CuO NPs. The FTIR spectrum of chitosan in comparison to the nCuO-CSs is displayed in Fig. 2b. The broad band around 3700–3000 cm^{-1} is associated with the overlapping of N–H and O–H stretching vibrations and the presence of intermolecular hydrogen bonds. The two peaks at ~2850–2950 cm^{-1} are characteristic to C–H stretching vibrations. The peak at 1652 cm^{-1} corresponds to C=O stretching of the amide group (the so-called amide I band) deriving from the *N*-acetyl-D-glucosamine moieties, while the peak at 1558 cm^{-1} represents N–H bending vibrations in the amide (amide II band) and amine groups. The peaks at 1417 and 1374 cm^{-1} are attributed to C–H bending in the methyl group of the amide, and the peak at 1311 cm^{-1} represents N–H bending and C–N stretching of the amide (amide III band). C–O stretching vibrations in the chitosan molecule are referred to by the peaks at 1150 and 894 cm^{-1}. The peak at 1058 cm^{-1} is associated with C3–OH stretching vibrations in the secondary alcohol, whereas the peak at 1023 cm^{-1} depicts C6–OH vibrations in the primary alcohol [38]. The aforementioned results were mostly in line with the research by Branca et al. [39] and Bujňáková et al. [38]. Finally, the peaks in the range of 500–600 cm^{-1} are representative of Cu–O stretching vibrations [40,41].

The interactions between chitosan and nanoparticles and/or ions are usually attributed to the –NH and –OH functional groups [38,39]. Hence, the corresponding peaks were taken under additional scrutiny. Compared to chitosan, the broad band around 3700–3000 cm^{-1} has increased in intensity for the nCuO-CS_1 and nCuO-CS_3 samples. A similar tendency, accompanied by a slight blueshift, is observable for the peaks representing the C3–OH and C6–OH vibrations (1100–1000 cm^{-1}).

3.3. XPS analysis

A full survey spectra (Fig. 2c) and narrow scans of Cu 2p (Fig. 2d), O 1s, C 1s, and N 1s (Fig. S3) were collected to determine the surface characteristics and chemical composition of the nCuO-CSs, chitosan was used for comparison. The survey spectra confirmed the presence of Cu in all NC samples (Table S2) and the absence of elemental impurities. Copper content was noticeably lower for the surface (1.0–3.2 at%) of the nCuO-CSs than the 'bulk samples' (10.7–17.0 at%; as determined by EDS). As expected, a decrease in the atomic concentration of Cu was observed for nCuO-CSs with a lower Cu:CS ratio, while the opposite was evident for carbon, indicating that the chitosan matrix surrounding the CuO particles varied in thickness, as presumed.

The C 1s spectra consist of three distinctive signals at 284.8, 286.2–286.5, and 288.1–288.6 eV. The signal at 284.8 eV can be attributed to C–C or C–H carbon species, the binding energy (BE) of 286.2–286.5 eV is associated with C–OH, C–N, or C–O–C bonding, and the signal at 288.1–288.6 eV is characteristic of the C=O or O–C–O bond [42–44]. The O 1s spectra reveal two distinctive maxima at 531.7–532.7 and 532.8–533.4 eV, which are representative of C–O and –OH functional groups, respectively. In the presence of copper, an extra peak was observed at BEs of 530.4–530.6 eV, associated with bonds in the oxide lattice [43]. This peak was not observed in the nCuO-CS_3 spectrum, probably due to minor Cu concentration (in relation to chitosan) and limits of the penetration signal. The N 1s spectrum of chitosan shows peaks for C–NH and C–N species. The former is absent from the nCuO-CSs spectra, possibly referring to charge transfer from nitrogen to copper that occurs when copper binds to chitosan [42].

Table 1
The physicochemical characteristics of chitosan-copper oxide nanocomposites (nCuO-CS) in deionized water. The dynamic light scattering and electrophoretic light scattering analyses were conducted at a concentration of ~40 mg Cu/L.

Sample	Cu:CS mass ratio	Hydrodynamic size, nm	ζ-potential, mV	PDI[a]
nCuO-CS_0.3	1:0.3	88 ± 6	+45.5 ± 0.6	0.23 ± 0.04
nCuO-CS_1	1:1	124 ± 20	+44.9 ± 1.1	0.27 ± 0.04
nCuO-CS_3	1:3	182 ± 2	+44.6 ± 0.1	0.33 ± 0.08
	Dissolved Cu per 1 mg Cu/L, %		Dissolved Cu per 10 mg Cu/L, %	
	1 h	24 h	1 h	24 h
nCuO-CS_0.3	19.4 ± 1.7	22.9 ± 0.3	2.7 ± 0.4	2.3 ± 0.9
nCuO-CS_1	19.0 ± 4.9	30.5 ± 6.7	2.7 ± 0.4	2.7 ± 0.8
nCuO-CS_3	16.1 ± 2.4	24.7 ± 7.2	2.9 ± 0.8	2.3 ± 1.2

[a] PDI – polydispersity index.

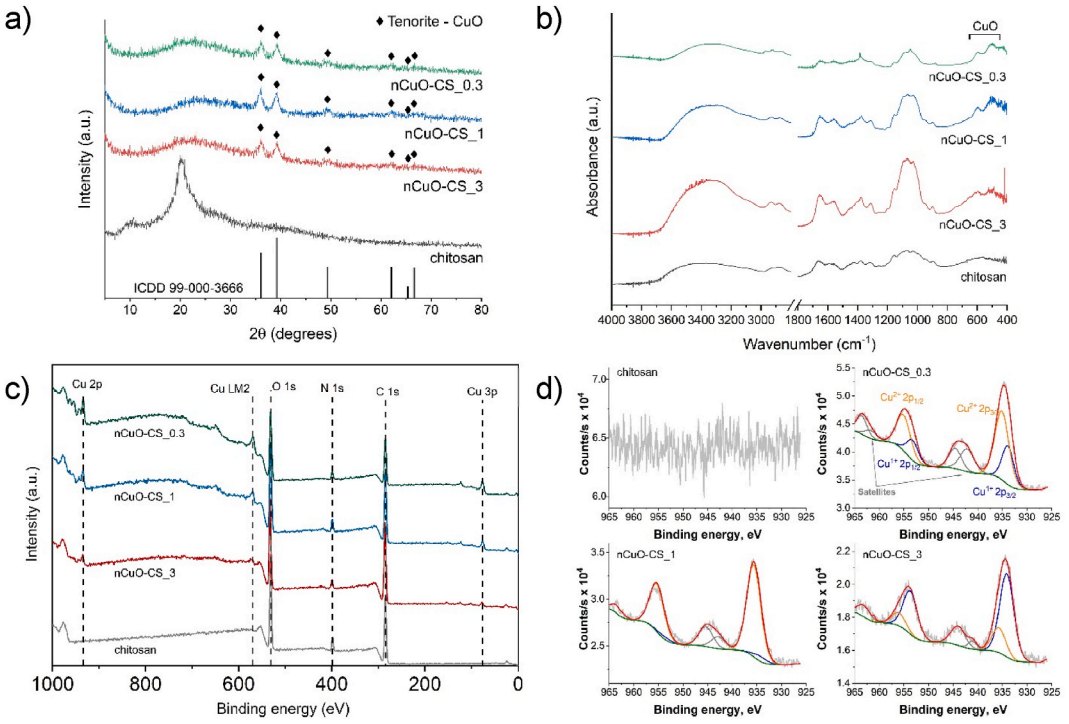

Fig. 2. Physicochemical properties of chitosan-copper oxide nanocomposites (nCuO-CS). (a) XRD spectra of chitosan and nCuO-CSs. (b) FTIR spectra of chitosan and nCuO-CSs. (c) XPS full survey spectra of chitosan and nCuO-CSs. (d) XPS narrow scan Cu 2p spectra of chitosan and nCuO-CSs. nCuO-CS_0.3, nCuO-CS_1, and nCuO-CS_3 designate different Cu:chitosan mass ratios (1:0.3, 1:1, and 1:3, respectively). The nCuO-CSs solutions were lyophilized prior to analyses.

The Cu 2p spectra (Fig. 2d) reveal the presence of both Cu(II) (fully coordinated) and Cu(I) (partially coordinated) species. Shake-up satellite peaks on the high BE side of primary peaks are typical of Cu(II) species, including CuO [43,45]. An increase in the Cu(II) signal can be seen for nCuO-CSs with a higher Cu:CS ratio. However, the proportion of Cu(II) to Cu(I) varies erratically between the nCuO-CSs. It might result from slightly different synthesis conditions, i.e., the NaOH amount was adjusted according to the used Cu:CS ratio. What is more, Basumallick et al. [44] noted the reduction of Cu(II) to Cu(I) in the presence of chitosan. Still, the latter does not explain why the prevalent Cu species detected in nCuO-CS_1 is Cu(II).

3.4. Shedding of copper ions

The release of copper ions is widely recognized as the prevalent mechanism underlying the toxicity of copper-based NPs [46,47]. In this study, the dissolution of copper ions from nCuO-CSs was quantified at two NC concentrations, 1 and 10 mg Cu/L, after 1- and 24-h incubation at 30 °C in DI water. Table 1 lists the percentages of dissolved Cu per nCuO-CSs. In general, 20–30 % of total copper was leached as Cu ions from the nCuO-CSs suspensions with 1 mg Cu/L and 2–3% from the samples with 10 mg Cu/L. Thus, the Cu:CS ratio in nCuO-CSs did not seem to impact the extent of copper dissolution in DI water. Literature data on the solubility of CuO-chitosan nanomaterials is scarce. However, under similar experimental conditions, Kasemets et al. [48] reported solubility rates of ~24 % and ~5 % for CuO NP suspensions at 1.6 and 16 mg Cu/L, respectively. Our results align with these findings, suggesting a comparable behavior of copper ion dissolution from the studied nCuO-CSs.

3.5. Antibacterial efficacy of chitosan-copper oxide nanocomposites

The cell viability test ('spot test') was used to determine the antibacterial efficacy of the nCuO-CSs. In parallel, the toxic effects of Cu^{2+} ions, chitosan (50–190 kDa), and commercial CuO NPs were analyzed (Table S3). Minimum biocidal concentration (MBC) was determined for *S. aureus* ATCC 6538, *P. aeruginosa* ATCC 27853, and two *E. coli* strains, MG1655 (with an inherently poor biofilm-forming ability [49,50]) and ATCC 25922 (biofilm-forming strain [51]). According to the 'spot test' results (Fig. 3, Table S3), *E. coli* MG1655 was initially more susceptible to the nCuO-CSs than *E. coli* ATCC 25922. In general, the results showed that after a 1-h exposure, the nCuO-CSs were about twice as toxic to Gram-negative bacteria (0.25–1.5 mg Cu/L) as Cu^{2+} ions (0.9–3.2 mg Cu/L), implying that chitosan may promote the interaction of nCuO-CSs and bacterial cells, facilitating the shedding of copper ions in their proximity and/or inducing membrane disturbances. Indeed, the polycationic chitosan is thought to bind the negatively charged components of the bacterial cell wall (e.g., lipopolysaccharides, teichoic acids) [52]. Moreover, the relative thinness of the

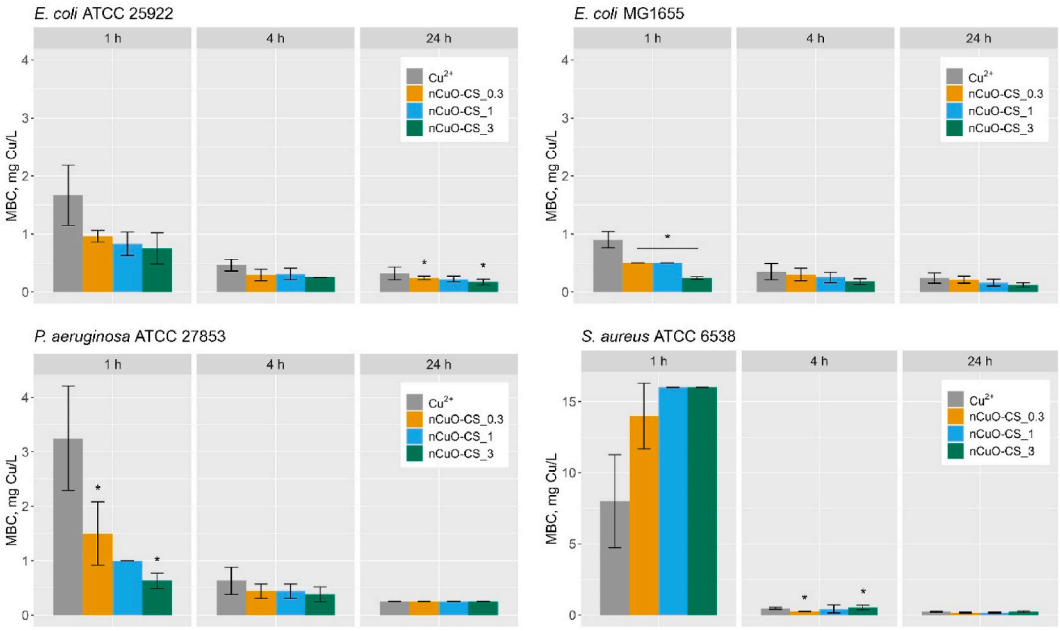

Fig. 3. The minimum biocidal concentration (MBC) of chitosan-copper oxide nanocomposites (nCuO-CSs) and copper(II) acetate (Cu^{2+}). All concentrations are nominal. Average values of at least three replicates are presented. MBC is the exposure concentration of the toxicant that did not yield viable bacterial growth after plating onto toxicant-free LB agar plates and the following incubation at 30 °C for 24 h nCuO-CS_0.3, nCuO-CS_1, and nCuO-CS_3 label different Cu:chitosan mass ratios (1:0.3, 1:1, and 1:3, respectively). Numerical MBC values are presented in Table S3. Asterisks designate statistically significant differences (*$p < 0.05$), which, for *E. coli* MG1655 (1-h MBC), were identified between nCuO-CS_1 and nCuO-CS_3 besides nCuO-CS_0.3 and nCuO-CS_3.

Gram-negative cell wall and outer cell membrane may leave them vulnerable to antibacterials targeting their surface.

Our initial hypothesis was that by increasing the proportion of chitosan, the antibacterial efficacy of the nCuO-CSs would also improve. However, the toxicity of the nCuO-CSs varied only slightly in conjunction with changes to the Cu:CS mass ratio. Statistically significant differences were identified between nCuO-CS_0.3 and nCuO-CS_3 for *E. coli* ATCC 25922 (24-h MBC), *E. coli* MG1655, *P. aeruginosa* (1-h MBC), and *S. aureus* (4-h MBC); and between nCuO-CS_1 and nCuO-CS_3 for *E. coli* MG1655 (1-h MBC). The commercial CuO NPs were initially substantially less toxic, with MBC values > 160 and > 6.5 mg Cu/L, after 1- and 4-h exposure, respectively (Table S3). After 24-h exposure, the toxicity of CuO NPs was ~1.0–2.9 mg Cu/L. These CuO NPs were chosen for comparison since they lack surface modification, and the results obtained help illustrate the role of chitosan in the antibacterial efficacy of the nCuO-CSs. Still, the authors note that these NPs are produced for a wide array of applications and likely excel in various areas.

During the first hour of exposure, the nCuO-CSs were less toxic than Cu^{2+} ions (~15 and 8.0 mg Cu/L, respectively) against the Gram-positive *S. aureus*, while chitosan was toxic (250 mg/L) only after 24-h exposure. As characteristic of Gram-positive bacteria, *S. aureus* has a thick peptidoglycan cell wall (~19 nm [53]), which may grant lower sensitivity against various toxicants. Yet interestingly, in 4 h, the toxicity of the nCuO-CSs toward *S. aureus* increased by two orders of magnitude, reaching levels comparable to those displayed against Gram-negative bacteria (4-h MBC ~0.5 mg Cu/L). Similarly, after 24-h exposure, the nCuO-CSs were equally potent toward Gram-negative and Gram-positive bacteria, acting at ~0.25 mg Cu/L MBC level. As the change in the amount of copper leached from the nCuO-CSs over the tested period was rather minor, such an increase in toxicity probably resulted from multiple factors. Recently, Liu et al. [7] described the antibacterial application of self-assembled Cu tannic acid NPs. They report a valence shift of copper (Cu^{2+} to Cu^{+}) caused by tannic acid, which was found to drive the toxicity of the NPs against *S. aureus*. In the current study, the presence of Cu_2O in addition to CuO might partially explain why the nCuO-CSs were uniformly toxic against all the tested bacteria. Indeed, the toxicity of Cu_2O is well documented [54–57]. The main difference between Gram-positive and Gram-negative bacteria was observed in respect to the antibacterial properties of chitosan (50–190 kDa), as it was less toxic to the Gram-positive *S. aureus* than the Gram-negative *E. coli* and *P. aeruginosa* (Table S3). The synergistic effect of chitosan and copper was most clearly demonstrated with *E. coli* MG1655 and *P. aeruginosa* after a 1-h exposure to the nCuO-CSs, as nCuO-CS_3 was about twice as toxic as nCuO-CS_0.3.

Data detailing the antibacterial properties of chitosan-copper oxide nanomaterials is scarce. Still, the zone of inhibition test has been used to assess [34,58–61] the antibacterial potential of various CS-CuO nanostructures, and the results support the current research. In a thorough study, Javed et al. [34] tested the antibacterial efficacy of chitosan-capped CuO NPs toward eight bacterial strains, including *S. aureus* (and the methicillin-resistant strain, MRSA), *P. aeruginosa*, and *E. coli*. They found the NPs similarly effective against all the tested bacteria (with inhibition zones of 8–11 mm) [34]. Bejan et al. [62] reduced the viability of *S. aureus* and *K. pneumoniae* by >85 % by applying CS nanofibers encapsulating CuO NPs. Additionally, various plant extracts (e.g., *Punica granatum*, *Sida cordifolia*) have been proposed [63,64] to improve the antimicrobial potency of CS-CuO nanocomposites.

3.6. Bioavailable copper

The bioavailable copper released from the nCuO-CSs was quantified using a Cu-inducible recombinant bioluminescent sensor bacteria, *E. coli* MC1061(pSLcueR/pDNPcopAlux), after 1- and 2-h exposure. Additionally, a control bacteria, *E. coli* MC1061(pDNlux), constitutively bioluminescent (not inducible by Cu ions), was employed to evaluate the toxicity of $CuSO_4$ and nCuO-CSs.

Luminescence of the sensor bacteria was induced by Cu ions in a concentration-dependent manner within the sub-toxic range of 0.0002–3.33 mg Cu/L (Fig. S4). Control bacteria data indicated that 1- and 2-h EC_{20} values (the concentration causing 20 % inhibition of bioluminescence) for $CuSO_4$ ranged from 3.01 to 3.56 mg Cu/L (Fig. S5). nCuO-CS_0.3, nCuO-CS_1 and nCuO-CS_3 led to 20 % inhibition of bioluminescence after 1- and 2-h exposure at concentrations of 0.72–0.98, 0.32–0.45, and 0.11–0.12 mg Cu/L, respectively (Fig. S6). The bioavailable copper released from the nCuO-CSs was quantified within the subtoxic range of 0.002–0.0625 mg Cu/L for all the studied nCuO-CSs.

Quantifying the bioavailability of Cu revealed that copper became bioavailable from the nCuO-CSs to the sensor bacteria already after a 1-h exposure (Fig. 4). The bioavailability of copper following a 1-h exposure was between 22 and 28 %. Notably, these values reached 45–66 % (Fig. 4, S6) after 2-h exposure. The bioavailability of Cu was higher than anticipated based on the solubility data of nCuO-CSs under abiotic conditions. Specifically, after 1- and 24-h incubation, the solubility of nCuO-CSs in DI water at a concentration of 1 mg Cu/L was 16–19 % and 22–30 %, respectively (Table 1).

One possible explanation for the increased bioavailability is the enhanced solubility of nCuO-CSs near the cell surface, facilitated by particle-cell interactions. Given that the tested nCuO-CSs exhibited a ζ-potential of approximately +45 mV (Table 1), these nanocomposites are expected to readily bind to bacteria, enhancing their bioavailability and antibacterial efficiency.

A comparison of copper bioavailability with varying Cu to chitosan ratios showed initial similarity across nCuO-CSs after a 1-h exposure. However, after 2 h, the bioavailable copper from nCuO-CSs at a concentration of 0.016 mg Cu/L was 47.2 (nCuO-CS_0.3), 56.7 (nCuO-CS_1), and 65.7 % (nCuO-CS_3), indicating higher bioavailability with increased CS concentration (Fig. S6).

3.7. Reactive oxygen species

The generation of ROS and the ensuing oxidative stress is often reported as the primary bactericidal mechanism of Cu ions (and those leached from copper-based NPs), yet data from different studies are inconclusive, even contradictory. Evidence in support of ROS generation as the key contributor toward copper's antimicrobial activity [7,56,65–67] is confronted by research demonstrating the opposite [31,57,68–70]. Furthermore, data supporting an alternative pathway involving the iron-sulfur (Fe–S) proteins has recently been increasing – excess intracellular copper seems to successfully compete with iron for its binding site in the Fe–S clusters, leading to the disintegration of the protein or inhibition of its biosynthesis [71–74]. The Fe–S clusters have various physiological functions (for a comprehensive review, the reader is directed to Ref. [75]), and disturbances in their operation can have a detrimental effect. Still, data in favor of ROS-induced toxicity is also accumulating [7,56], indicating that multiple mechanisms are likely involved.

Furthermore, Shi et al. [76] found that ROS generation can vary depending on NP surface modifications. Hence, we conducted assays in both abiotic and biotic conditions to determine whether the toxicity of the nCuO-CSs was associated with ROS generation. $DCFH_2$-DA, a well-known [77] fluorescent probe for ROS measurement, was used in both experiments. The tests were performed with nCuO-CSs concentrations ranging from 0.01 to 10 mg Cu/L, the former being below and the latter above the determined 24-h MBC values for all the studied bacteria. No ROS generation was detected (Fig. S7) for the nCuO-CSs compared to the negative control (DI water) in neither biotic nor abiotic conditions. Since increased ROS production was observed after treatment with the positive controls, Mn_3O_4 NPs (abiotic conditions) and H_2O_2 (biotic), the nCuO-CSs probably acted through a different bactericidal mechanism.

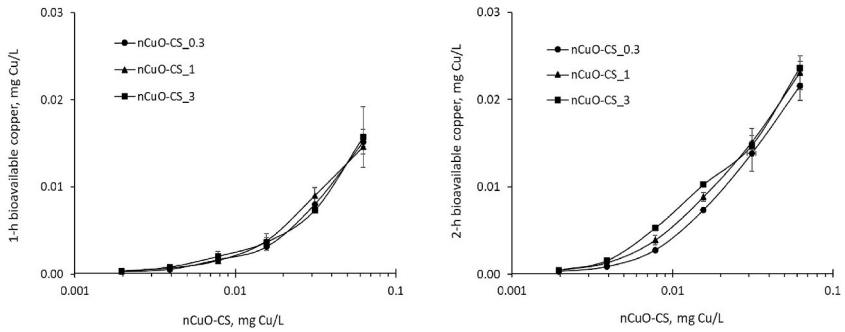

Fig. 4. Bioavailable copper (Cu^{2+}) released from the chitosan-copper oxide nanocomposites with Cu:chitosan weight ratios of 1:0.3 (nCuO-CS_0.3), 1:1 (nCuO-CS_1), and 1:3 (nCuO-CS_3) after 1-h and 2-h incubation at 30 °C. Bioavailable copper was quantified using recombinant luminescent Cu-inducible bacteria *E. coli* MC1061(pSLcueR/PDNPcopAlux) in an induction medium composed of 20 mM MOPS (pH 6.5), 0.05 % acid hydrolyzed casein, and 0.05 % glucose.

3.8. Bacterial cell-to-nanocomposite interactions

Confocal laser scanning microscopy (CLSM) and flow cytometry analyses were performed to investigate the interactions between nCuO-CSs and bacteria. CLSM images show that exposure to the nCuO-CSs seemed to cause the clamping of bacterial cells (Fig. 5, S8, S9). This clustering was pronounced for *E. coli* MG1655 with all studied nCuO-CSs, for *E. coli* ATCC 25922 with nCuO-CS_1 and nCuO-CS_3, and for *P. aeruginosa* with nCuO-CS_3 (all nCuO-CSs were tested at 1 mg Cu/L). This effect was not observable for *S. aureus* at 1 mg Cu/L but was apparent at 10 mg Cu/L (close to the MBC of the nCuO-CSs against *S. aureus* after a 1-h exposure, Table S3). In general, the flow cytometry analyses at toxic concentrations were in line with these observations (i.e., a shift in side scatter intensity was observed only for *P. aeruginosa* with nCuO-CS_0.3 and nCuO-CS_1 at 1 mg Cu/L, Fig. S10). To a lesser degree, the tendency to clamp was also evident with exposure to chitosan (tested at 1 and 3 mg/L, Fig. S11; additionally tested at 10 and 30 mg/L with *S. aureus*, Fig. S9), and with regards to the latter, has been documented before [78]. However, it is important to note that unlike in the synthesis of the nCuO-CSs, chitosan evaluated in CLSM studies did not undergo heating nor alkali treatment. Disruption of the bacterial cell membrane and the formation of a polymeric barrier around bacteria, restricting nutrient uptake, are among the proposed bactericidal mechanisms of chitosan [24]. The clamping effect observed in this work is possibly connected to chitosan-facilitated nanocomposite adsorption to the surface of bacteria, followed by membrane disruption [79]. Hence, these interactions could partly explain why the nCuO-CSs were at first more toxic to Gram-negative bacteria than Cu^{2+} ions.

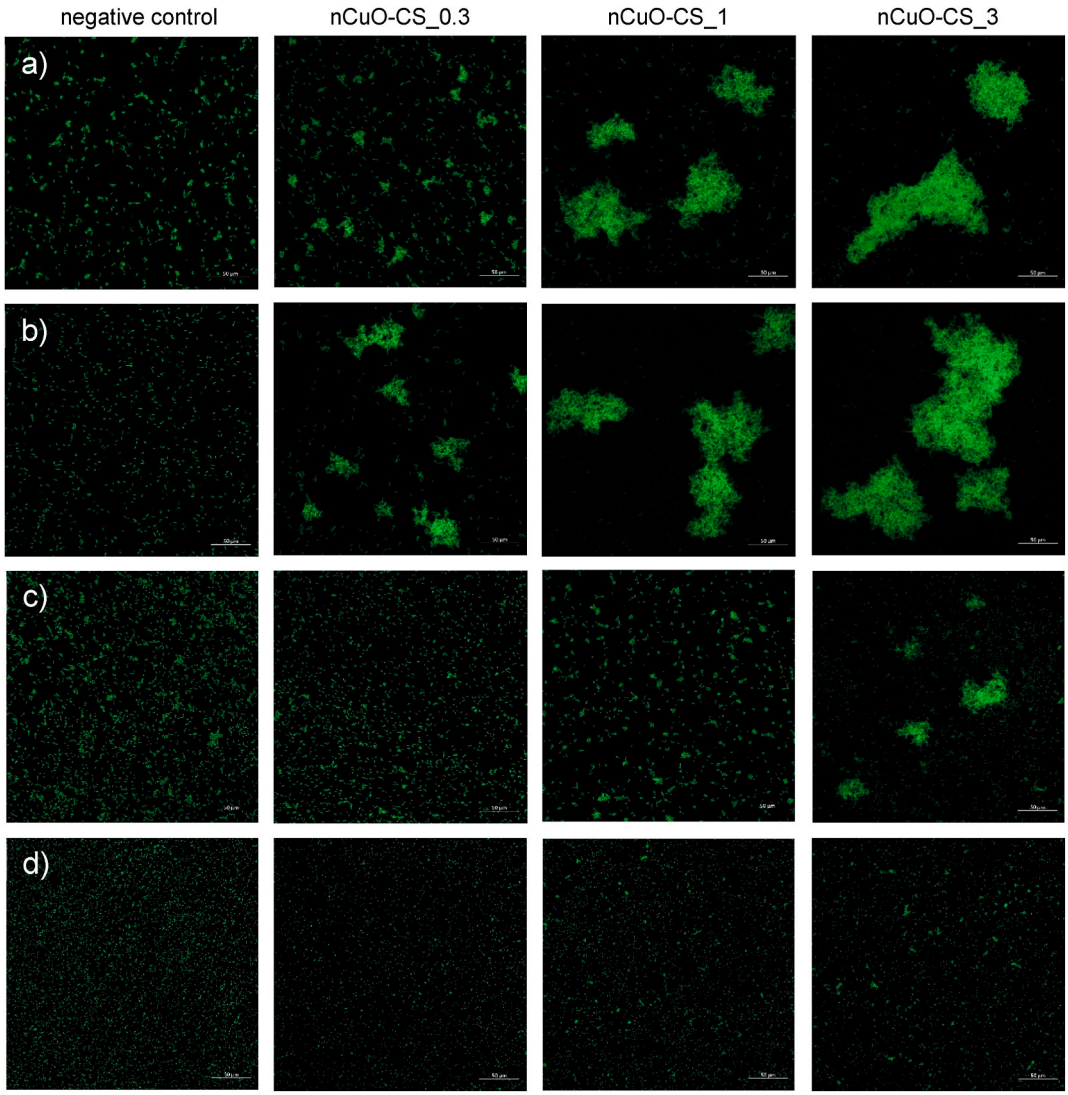

Fig. 5. Confocal laser scanning microscopy images of bacterial cells. (a) *Escherichia coli* ATCC 25922, (b) *E. coli* MG1655, (c) *Pseudomonas aeruginosa* ATCC 27853, and (d) *Staphylococcus aureus* ATCC 6538 were exposed to chitosan-copper oxide nanocomposites (nCuO-CS) in deionized water at a concentration of 1 mg Cu/L for 1 h at 30 °C in the dark. nCuO-CS_0.3, nCuO-CS_1, and nCuO-CS_3 designate nanocomposites with different Cu: chitosan mass ratios (1:0.3, 1:1, and 1:3, respectively). All scale bars are 50 μm.

In addition, the impact of the nCuO-CSs on the integrity of the bacterial cell membrane was explored. Propidium iodide, which penetrates only cells with damaged membranes, was used alongside SYTO 9 (the latter can enter both damaged and intact cells) to stain cells after a 1-h exposure to the nCuO-CSs (tested at 1 mg Cu/L). The CLSM images (Figs. S12 and S13) show evidence of membrane damage, but since the cells were not stained red uniformly (at the ~1-h MBC level), suggest that multiple mechanisms are involved. For comparison, all cells stained red upon treatment with the positive control, sodium dodecyl sulfate (at 1 g/L). As detailed in section 3.6., exposure to the nCuO-CSs also increased cell bioavailable copper. Thus, the proposed overall bactericidal effect likely starts with the adsorption of nCuO-CSs onto the surface of bacteria, followed by an increase in cell bioavailable copper, membrane damage and/or cell clamping.

3.9. Conclusions

To conclude, a facile precipitation method for the synthesis of chitosan-copper oxide nanocomposites (nCuO-CSs) was modified, yielding stable colloidal suspensions. The nCuO-CSs were found to be agglomerates of up to 100 nm, composed of particles with a primary size of ~10 nm, and had a ζ-potential of >+40 mV. After 4 h, toxicity (4-h MBC 0.25–0.5 mg Cu/L) was similar against all the tested bacteria, the Gram-negative *E. coli* and *P. aeruginosa*, and the Gram-positive *S. aureus*. However, against Gram-negative bacteria, this inhibitory effect was already evident after a 1-h exposure and surpassed that of copper ions, implying to a synergistic effect of chitosan and nano-CuO. Using flow cytometry and confocal laser scanning microscopy, we showed that chitosan promoted interaction between the nCuO-CSs and bacterial cells, possibly resulting in increased cell bioavailable copper and/or membrane damage. Indeed, the increase in bioavailable copper was confirmed by a biosensor (Cu-sensing recombinant bacteria) assay. At the same time, propidium iodide staining suggests that the nCuO-CSs also provoke membrane damage. Taken together, the bactericidal mechanism of the nCuO-CSs likely results from a combined effect of multiple stressors. The synergy between copper and chitosan makes these nanomaterials promising for biomedical applications (e.g., wound dressings). Still, to rule out possible adverse effects to humans and to determine the therapeutic window, the nCuO-CSs should next be evaluated in thorough cytotoxicity analyses.

Data availability

Data will be made available on request.

CRediT authorship contribution statement

Jüri Laanoja: Writing – review & editing, Writing – original draft, Visualization, Methodology, Investigation, Formal analysis, Conceptualization. **Mariliis Sihtmäe:** Writing – review & editing, Methodology, Formal analysis. **Svetlana Vihodceva:** Writing – review & editing, Methodology, Formal analysis. **Mairis Iesalnieks:** Writing – review & editing, Methodology, Formal analysis. **Maarja Otsus:** Writing – review & editing, Methodology, Investigation, Formal analysis. **Imbi Kurvet:** Methodology, Investigation, Formal analysis. **Anne Kahru:** Writing – review & editing, Writing – original draft, Investigation, Conceptualization. **Kaja Kasemets:** Writing – review & editing, Writing – original draft, Visualization, Methodology, Investigation, Funding acquisition, Formal analysis, Conceptualization.

Declaration of competing interest

The authors declare that they have no known competing financial interests or personal relationships that could have appeared to influence the work reported in this paper.

Acknowledgements

This work was supported by the Estonian Research Council projects PRG749, TEM-TA55 and the NAMUR+ core facility (TT13). The authors thank Heiki Vija for his advice and support.

Appendix A. Supplementary data

Supplementary data to this article can be found online at https://doi.org/10.1016/j.heliyon.2024.e35588.

References

[1] Antimicrobial resistance, (n.d.). https://www.who.int/news-room/fact-sheets/detail/antimicrobial-resistance (accessed February 4, 2024).
[2] A.J. Browne, M.G. Chipeta, G. Haines-Woodhouse, E.P.A. Kumaran, B.H.K. Hamadani, S. Zaraa, N.J. Henry, A. Deshpande, R.C. Reiner, N.P.J. Day, A.D. Lopez, S. Dunachie, C.E. Moore, A. Stergachis, S.I. Hay, C. Dolecek, Global antibiotic consumption and usage in humans, 2000–18: a spatial modelling study, Lancet Planet. Health 5 (2021) e893–e904, https://doi.org/10.1016/S2542-5196(21)00280-1.
[3] Infographic: healthcare-associated infections – a threat to patient safety in Europe. https://www.ecdc.europa.eu/en/publications-data/infographic-healthcare-associated-infections-threat-patient-safety-europe, 2018. (Accessed 4 February 2024).

[4] C.J.L. Murray, K.S. Ikuta, F. Sharara, L. Swetschinski, G. Robles Aguilar, A. Gray, C. Han, C. Bisignano, P. Rao, E. Wool, S.C. Johnson, A.J. Browne, M.G. Chipeta, F. Fell, S. Hackett, G. Haines-Woodhouse, B.H. Kashef Hamadani, E.A.P. Kumaran, B. McManigal, S. Achalapong, R. Agarwal, S. Akech, S. Albertson, J. Amuasi, J. Andrews, A. Aravkin, E. Ashley, F.-X. Babin, F. Bailey, S. Baker, B. Basnyat, A. Bekker, R. Bender, J.A. Berkley, A. Bethou, J. Bielicki, S. Boonkasidecha, J. Bukosia, C. Carvalheiro, C. Castañeda-Orjuela, V. Chansamouth, S. Chaurasia, S. Chiurchiù, F. Chowdhury, R. Clotaire Donatien, A.J. Cook, B. Cooper, T. R. Cressey, E. Criollo-Mora, M. Cunningham, S. Darboe, N.P.J. Day, M. De Luca, K. Dokova, A. Dramowski, S.J. Dunachie, T. Duong Bich, T. Eckmanns, D. Eibach, A. Emami, N. Feasey, N. Fisher-Pearson, K. Forrest, C. Garcia, D. Garrett, P. Gastmeier, A.Z. Giref, R.C. Greer, V. Gupta, S. Haller, A. Haselbeck, S. I. Hay, M. Holm, S. Hopkins, Y. Hsia, K.C. Iregbu, J. Jacobs, D. Jarovsky, F. Javanmardi, A.W.J. Jenney, M. Khorana, S. Khusuwan, N. Kissoon, E. Kobeissi, T. Kostyanev, F. Krapp, R. Krumkamp, A. Kumar, H.H. Kyu, C. Lim, K. Lim, D. Limmathurotsakul, M.J. Loftus, M. Lunn, J. Ma, A. Manoharan, F. Marks, J. May, M. Mayxay, N. Mturi, T. Munera-Huertas, P. Musicha, L.A. Musila, M.M. Mussi-Pinhata, R.N. Naidu, T. Nakamura, R. Nanavati, S. Nangia, P. Newton, C. Ngoun, A. Novotney, D. Nwakanma, C.W. Obiero, T.J. Ochoa, A. Olivas-Martinez, P. Olliaro, E. Ooko, E. Ortiz-Brizuela, P. Ounchanum, G.D. Pak, J.L. Paredes, A. Y. Peleg, C. Perrone, T. Phe, K. Phommasone, N. Plakkal, A. Ponce-de-Leon, M. Raad, T. Ramdin, S. Rattanavong, A. Riddell, T. Roberts, J.V. Robotham, A. Roca, V.D. Rosenthal, K.E. Rudd, N. Russell, H.S. Sader, W. Saengchan, J. Schnall, J.A.G. Scott, S. Seekaew, M. Sharland, M. Shivamallappa, J. Sifuentes-Osornio, A. J. Simpson, N. Steenkeste, A.J. Stewardson, T. Stoeva, N. Tasak, A. Thaiprakong, G. Thwaites, C. Tigoi, C. Turner, P. Turner, H.R. Van Doorn, S. Velaphi, A. Vongpradith, M. Vongsouvath, H. Vu, T. Walsh, J.L. Walson, S. Waner, T. Wangrangsimakul, P. Wannapinij, T. Wozniak, T.E.M.W. Young Sharma, K.C. Yu, P. Zheng, B. Sartorius, A.D. Lopez, A. Stergachis, C. Moore, C. Dolecek, M. Naghavi, Global burden of bacterial antimicrobial resistance in 2019: a systematic analysis, Lancet 399 (2022) 629–655, https://doi.org/10.1016/S0140-6736(21)02724-0.

[5] C. Su, A.K. Berekute, K.-P. Yu, Chitosan@TiO2 composites for the adsorption of copper(II) and antibacterial applications, Sustain. Environ. Res. 32 (2022) 27, https://doi.org/10.1186/s42834-022-00138-7.

[6] M. Dadmehr, B. Korouzhdehi, A. Tavassoli, M. Malekkiani, Photocatalytic activity of green synthesized cadmium sulfide quantum dots on the removal of RhB dye and its cytotoxicity and antibacterial studies, Nanotechnology 33 (2022) 395101, https://doi.org/10.1088/1361-6528/ac79bc.

[7] T. Liu, M. Ma, A. Ali, Q. Liu, R. Bai, K. Zhang, Y. Guan, Y. Wang, J. Liu, H. Zhou, Self-assembled copper tannic acid nanoparticles: a powerful nano-bactericide by valence shift of copper, Nano Today 54 (2024) 102071, https://doi.org/10.1016/j.nantod.2023.102071.

[8] W.N. Dlamini, T.-C. Yao, H.-J. Lee, A.K. Berekute, R. Sallah-Ud-Din, S. Siregar, K.-P. Yu, Enhanced removal of viral aerosols using nanosilver/TiO2-chitosan filters combined with a negative air ionizer, J. Environ. Chem. Eng. 12 (2024) 112973, https://doi.org/10.1016/j.jece.2024.112973.

[9] M. Malekkiani, A.H.J. Magham, F. Ravari, M. Dadmehr, Enhanced ultraviolet driven photocatalytic activity of CTS-SnO2-MWCNTs ternary nanohybrid for photodegradation of methylene blue and bacteria in aqueous solutions, Environ. Technol. Innov. 34 (2024) 103559, https://doi.org/10.1016/j.eti.2024.103559.

[10] A. Nel, T. Xia, Toxic Potential of Materials at the Nanolevel, vol. 311, 2006.

[11] L. Yildirimer, N.T.K. Thanh, M. Loizidou, A.M. Seifalian, Toxicology and clinical potential of nanoparticles, Nano Today 6 (2011) 585–607, https://doi.org/10.1016/j.nantod.2011.10.001.

[12] N. Niño-Martínez, M.F. Salas Orozco, G.-A. Martínez-Castañón, F. Torres Méndez, F. Ruiz, Molecular mechanisms of bacterial resistance to metal and metal oxide nanoparticles, Int. J. Mol. Sci. 20 (2019) 2808, https://doi.org/10.3390/ijms20112808.

[13] N. Chakraborty, D. Jha, I. Roy, P. Kumar, S.S. Gaurav, K. Marimuthu, O.-T. Ng, R. Lakshminarayanan, N.K. Verma, H.K. Gautam, Nanobiotics against antimicrobial resistance: harnessing the power of nanoscale materials and technologies, J. Nanobiotechnol. 20 (2022) 1–25, https://doi.org/10.1186/s12951-022-01573-9.

[14] M. Xie, M. Gao, Y. Yun, M. Malmsten, V.M. Rotello, R. Zboril, O. Akhavan, A. Kraskouski, J. Amalraj, X. Cai, J. Lu, H. Zheng, R. Li, Antibacterial nanomaterials: mechanisms, impacts on antimicrobial resistance and design principles, Angew. Chem. Int. Ed. 62 (2023) e202217345, https://doi.org/10.1002/anie.202217345.

[15] A. Panáček, L. Kvítek, M. Smékalová, R. Večeřová, M. Kolář, M. Röderová, F. Dyčka, M. Šebela, R. Prucek, O. Tomanec, R. Zbořil, Bacterial resistance to silver nanoparticles and how to overcome it, Nat. Nanotechnol. 13 (2018) 65–71, https://doi.org/10.1038/s41565-017-0013-y.

[16] S. Zhang, Y. Wang, H. Song, J. Lu, Z. Yuan, J. Guo, Copper nanoparticles and copper ions promote horizontal transfer of plasmid-mediated multi-antibiotic resistance genes across bacterial genera, Environ. Int. 129 (2019) 478–487, https://doi.org/10.1016/j.envint.2019.05.054.

[17] V. Pareek, R. Gupta, S. Devineau, S.K. Sivasankaran, A. Bhargava, MohdA. Khan, S. Srikumar, S. Fanning, J. Panwar, Does silver in different forms affect bacterial susceptibility and resistance? A mechanistic perspective, ACS Appl. Bio Mater. 5 (2022) 801–817, https://doi.org/10.1021/acsabm.1c01179.

[18] O. Bondarenko, K. Juganson, A. Ivask, K. Kasemets, M. Mortimer, A. Kahru, Toxicity of Ag, CuO and ZnO nanoparticles to selected environmentally relevant test organisms and mammalian cells in vitro: a critical review, Arch. Toxicol. 87 (2013) 1181–1200, https://doi.org/10.1007/s00204-013-1079-4.

[19] A.P. Kornblatt, V.G. Nicoletti, A. Travaglia, The neglected role of copper ions in wound healing, J. Inorg. Biochem. 161 (2016) 1–8, https://doi.org/10.1016/j.jinorgbio.2016.02.012.

[20] J. Salvo, C. Sandoval, Role of copper nanoparticles in wound healing for chronic wounds: literature review, Burns Trauma 10 (2022) tkab047, https://doi.org/10.1093/burnst/tkab047.

[21] R. Javed, M. Zia, S. Naz, S.O. Aisida, N.U. Ain, Q. Ao, Role of capping agents in the application of nanoparticles in biomedicine and environmental remediation: recent trends and future prospects, J. Nanobiotechnol. 18 (2020) 172, https://doi.org/10.1186/s12951-020-00704-4.

[22] J. Jeevanandam, A. Barhoum, Y.S. Chan, A. Dufresne, M.K. Danquah, Review on nanoparticles and nanostructured materials: history, sources, toxicity and regulations, Beilstein J. Nanotechnol. 9 (2018) 1050–1074, https://doi.org/10.3762/bjnano.9.98.

[23] A. Saravanan, P.S. Kumar, D. Yuvaraj, S. Jeevanantham, P. Aishwaria, P.B. Gnanasri, M. Gopinath, G. Rangasamy, A review on extraction of polysaccharides from crustacean wastes and their environmental applications, Environ. Res. 221 (2023) 115306, https://doi.org/10.1016/j.envres.2023.115306.

[24] Aachmann Matica, Sletta Tøndervik, Ostafe, Chitosan as a wound dressing starting material: antimicrobial properties and mode of action, Int. J. Mol. Sci. 20 (2019) 5889, https://doi.org/10.3390/ijms20235889.

[25] G. Kravanja, M. Primožič, Ž. Knez, M. Leitgeb, Chitosan-based (Nano)Materials for novel biomedical applications, Molecules 24 (2019) 1960, https://doi.org/10.3390/molecules24101960.

[26] P. Feng, Y. Luo, C. Ke, H. Qiu, W. Wang, Y. Zhu, R. Hou, L. Xu, S. Wu, Chitosan-based functional materials for skin wound repair: mechanisms and applications, Front. Bioeng. Biotechnol. 9 (2021) 650598, https://doi.org/10.3389/fbioe.2021.650598.

[27] X. Wang, R. Song, M. Johnson, S. A, P. Shen, N. Zhang, I. Lara-Sáez, Q. Xu, W. Wang, Chitosan-based hydrogels for infected wound treatment, Macromol. Biosci. 23 (2023) 2300094, https://doi.org/10.1002/mabi.202300094.

[28] A.A. Gvozdenko, S.A. Siddiqui, A.V. Blinov, A.B. Golik, A.A. Nagdalian, D.G. Maglakelidze, E.N. Statsenko, M.A. Pirogov, A.A. Blinova, M.N. Sizonenko, A. N. Simonov, R.B. Zhukov, R.O. Kolesnikov, S.A. Ibrahim, Synthesis of CuO nanoparticles stabilized with gelatin for potential use in food packaging applications, Sci. Rep. 12 (2022) 12843, https://doi.org/10.1038/s41598-022-16878-w.

[29] S. Suppi, K. Kasemets, A. Ivask, K. Künnis-Beres, M. Sihtmäe, I. Kurvet, V. Aruoja, A. Kahru, A novel method for comparison of biocidal properties of nanomaterials to bacteria, yeasts and algae, J. Hazard Mater. 286 (2015) 75–84, https://doi.org/10.1016/j.jhazmat.2014.12.027.

[30] M. Heinlaan, A. Ivask, I. Blinova, H.-C. Dubourguier, A. Kahru, Toxicity of nanosized and bulk ZnO, CuO and TiO2 to bacteria *Vibrio fischeri* and crustaceans *Daphnia magna* and *Thamnocephalus platyurus*, Chemosphere 71 (2008) 1308–1316, https://doi.org/10.1016/j.chemosphere.2007.11.047.

[31] V. Aruoja, S. Pokhrel, M. Sihtmäe, M. Mortimer, L. Mädler, A. Kahru, Toxicity of 12 metal-based nanoparticles to algae, bacteria and protozoa, Environ. Sci.: Nano 2 (2015) 630–644, https://doi.org/10.1039/C5EN00057B.

[32] S. Käosaar, A. Kahru, P. Mantecca, K. Kasemets, Profiling of the toxicity mechanisms of coated and uncoated silver nanoparticles to yeast Saccharomyces cerevisiae BY4741 using a set of its 9 single-gene deletion mutants defective in oxidative stress response, cell wall or membrane integrity and endocytosis, Toxicol. Vitro 35 (2016) 149–162, https://doi.org/10.1016/j.tiv.2016.05.018.

[33] Z.V. Feng, I.L. Gunsolus, T.A. Qiu, K.R. Hurley, L.H. Nyberg, H. Frew, K.P. Johnson, A.M. Vartanian, L.M. Jacob, S.E. Lohse, M.D. Torelli, R.J. Hamers, C. J. Murphy, C.L. Haynes, Impacts of gold nanoparticle charge and ligand type on surface binding and toxicity to Gram-negative and Gram-positive bacteria, Chem. Sci. 6 (2015) 5186–5196, https://doi.org/10.1039/C5SC00792E.

[34] R. Javed, F. Rais, M. Kaleem, B. Jamil, M.A. Ahmad, T. Yu, S.W. Qureshi, Q. Ao, Chitosan capping of CuO nanoparticles: facile chemical preparation, biological analysis, and applications in dentistry, Int. J. Biol. Macromol. 167 (2021) 1452–1467, https://doi.org/10.1016/j.ijbiomac.2020.11.099.

[35] S. Sonia, N.D. Jayram, P. Suresh Kumar, D. Mangalaraj, N. Ponpandian, C. Viswanathan, Effect of NaOH concentration on structural, surface and antibacterial activity of CuO nanorods synthesized by direct sonochemical method, Superlattices Microstruct 66 (2014) 1–9, https://doi.org/10.1016/j.spmi.2013.10.020.

[36] C.-L. Ke, F.-S. Deng, C.-Y. Chuang, C.-H. Lin, Antimicrobial actions and applications of chitosan, Polymers 13 (2021) 904, https://doi.org/10.3390/polym13060904.

[37] S. Bhattacharjee, DLS and zeta potential – what they are and what they are not? J. Contr. Release 235 (2016) 337–351, https://doi.org/10.1016/j.jconrel.2016.06.017.

[38] Z. Bujňáková, E. Dutková, A. Zorkovská, M. Baláž, J. Kováč, M. Kello, J. Mojžiš, J. Briančin, P. Baláž, Mechanochemical synthesis and in vitro studies of chitosan-coated InAs/ZnS mixed nanocrystals, J. Mater. Sci. 52 (2017) 721–735, https://doi.org/10.1007/s10853-016-0366-x.

[39] C. Branca, G. D'Angelo, C. Crupi, K. Khouzami, S. Rifici, G. Ruello, U. Wanderlingh, Role of the OH and NH vibrational groups in polysaccharide-nanocomposite interactions: a FTIR-ATR study on chitosan and chitosan/clay films, Polymer 99 (2016) 614–622, https://doi.org/10.1016/j.polymer.2016.07.086.

[40] M. Figiela, M. Wysokowski, M. Galinski, T. Jesionowski, I. Stepniak, Synthesis and characterization of novel copper oxide-chitosan nanocomposites for non-enzymatic glucose sensing, Sensor. Actuator. B Chem. 272 (2018) 296–307, https://doi.org/10.1016/j.snb.2018.05.173.

[41] N.B. Tanvir, O. Yurchenko, Ch Wilbertz, G. Urban, Investigation of CO_2 reaction with copper oxide nanoparticles for room temperature gas sensing, J. Mater. Chem. A 4 (2016) 5294–5302, https://doi.org/10.1039/C5TA09089J.

[42] L. Dambies, C. Guimon, S. Yiacoumi, E. Guibal, Characterization of metal ion interactions with chitosan by X-ray photoelectron spectroscopy, Colloids Surf. A Physicochem. Eng. Asp. 177 (2001) 203–214, https://doi.org/10.1016/S0927-7757(00)00678-6.

[43] F.C. De Godoi, E. Rodriguez-Castellon, E. Guibal, M.M. Beppu, An XPS study of chromate and vanadate sorption mechanism by chitosan membrane containing copper nanoparticles, Chem. Eng. J. 234 (2013) 423–429, https://doi.org/10.1016/j.cej.2013.09.006.

[44] S. Basumallick, P. Rajasekaran, L. Tetard, S. Santra, Hydrothermally derived water-dispersible mixed valence copper-chitosan nanocomposite as exceptionally potent antimicrobial agent, J. Nanoparticle Res. 16 (2014) 2675, https://doi.org/10.1007/s11051-014-2675-9.

[45] M.C. Biesinger, L.W.M. Lau, A.R. Gerson, R.StC. Smart, Resolving surface chemical states in XPS analysis of first row transition metals, oxides and hydroxides: Sc, Ti, V, Cu and Zn, Appl. Surf. Sci. 257 (2010) 887–898, https://doi.org/10.1016/j.apsusc.2010.07.086.

[46] I. Salah, I.P. Parkin, E. Allan, Copper as an antimicrobial agent: recent advances, RSC Adv. 11 (2021) 18179–18186, https://doi.org/10.1039/D1RA02149D.

[47] J. Ramos-Zúñiga, N. Bruna, J.M. Pérez-Donoso, Toxicity mechanisms of copper nanoparticles and copper surfaces on bacterial cells and viruses, Int. J. Mol. Sci. 24 (2023) 10503, https://doi.org/10.3390/ijms241310503.

[48] K. Kasemets, S. Suppi, K. Künnis-Beres, A. Kahru, Toxicity of CuO nanoparticles to yeast *Saccharomyces cerevisiae* BY4741 wild-type and its nine isogenic single-gene deletion mutants, Chem. Res. Toxicol. 26 (2013) 356–367, https://doi.org/10.1021/tx300467d.

[49] J.-M. Ghigo, Natural conjugative plasmids induce bacterial biofilm development, Nature 412 (2001) 442–445, https://doi.org/10.1038/35086581.

[50] A. Reisner, J.A.J. Haagensen, M.A. Schembri, E.L. Zechner, S. Molin, Development and maturation of Escherichia coli K-12 biofilms, Mol. Microbiol. 48 (2003) 933–946, https://doi.org/10.1046/j.1365-2958.2003.03490.x.

[51] M. Alshammari, A. Ahmad, M. AlKhulaifi, D. Al Farraj, S. Alsudir, M. Alarawi, G. Takashi, E. Alyamani, Reduction of biofilm formation of *Escherichia coli* by targeting quorum sensing and adhesion genes using the CRISPR/Cas9-HDR approach, and its clinical application on urinary catheter, J. Infect. Public Health 16 (2023) 1174–1183, https://doi.org/10.1016/j.jiph.2023.05.026.

[52] D. Raafat, K. von Bargen, A. Haas, H.-G. Sahl, Insights into the mode of action of chitosan as an antibacterial compound, Appl. Environ. Microbiol. 74 (2008) 3764–3773, https://doi.org/10.1128/AEM.00453-08.

[53] V.R.F. Matias, T.J. Beveridge, Native cell wall organization shown by cryo-electron microscopy confirms the existence of a periplasmic space in *Staphylococcus aureus*, J. Bacteriol. 188 (2006) 1011–1021, https://doi.org/10.1128/JB.188.3.1011-1021.2006.

[54] K. Sunada, M. Minoshima, K. Hashimoto, Highly efficient antiviral and antibacterial activities of solid-state cuprous compounds, J. Hazard Mater. 235–236 (2012) 265–270, https://doi.org/10.1016/j.jhazmat.2012.07.052.

[55] M. Hans, A. Erbe, S. Mathews, Y. Chen, M. Solioz, F. Mücklich, Role of copper oxides in contact killing of bacteria, Langmuir 29 (2013) 16160–16166, https://doi.org/10.1021/la404091z.

[56] D. Kong, C. Ma, W. Wang, C. Liu, Y. Tian, T. Wang, Z. Zhao, C. Zhang, H. Feng, S. Chen, Two birds with one stone: interfacial controls and pH response for long-term and high-efficiency Cu2O antibacterial materials, Chem. Eng. J. 427 (2022) 131734, https://doi.org/10.1016/j.cej.2021.131734.

[57] S. Behzadinasab, M.D. Williams, J.O. Falkinham Iii, W.A. Ducker, Antimicrobial mechanism of cuprous oxide (Cu2O) coatings, J. Colloid Interface Sci. 652 (2023) 1867–1877, https://doi.org/10.1016/j.jcis.2023.08.136.

[58] S. Farhoudian, M. Yadollahi, H. Namazi, Facile synthesis of antibacterial chitosan/CuO bio-nanocomposite hydrogel beads, Int. J. Biol. Macromol. 82 (2016) 837–843, https://doi.org/10.1016/j.ijbiomac.2015.10.018.

[59] H. Almasi, P. Jafarzadeh, L. Mehryar, Fabrication of novel nanohybrids by impregnation of CuO nanoparticles into bacterial cellulose and chitosan nanofibers: characterization, antimicrobial and release properties, Carbohydr. Polym. 186 (2018) 273–281, https://doi.org/10.1016/j.carbpol.2018.01.067.

[60] T. Jayaramudu, K. Varaprasad, R.D. Pyarasani, K.K. Reddy, K.D. Kumar, A. Akbari-Fakhrabadi, R.V. Mangalaraja, J. Amalraj, Chitosan capped copper oxide/copper nanoparticles encapsulated microbial resistant nanocomposite films, Int. J. Biol. Macromol. 128 (2019) 499–508, https://doi.org/10.1016/j.ijbiomac.2019.01.145.

[61] K. Parate, D. Meher, P. Gupta, P. Pandey, Chitosan-capped CuO nanoparticles: a comprehensive, comparative study of their broad-spectrum antibacterial efficacy, Appl. Nanosci. (2024), https://doi.org/10.1007/s13204-023-02987-z.

[62] A. Bejan, A. Anisiei, B.-I. Andreica, I. Rosca, L. Marin, Chitosan nanofibers encapsulating copper oxide nanoparticles: a new approach towards multifunctional ecological membranes with high antimicrobial and antioxidant efficiency, Int. J. Biol. Macromol. (2024) 129377, https://doi.org/10.1016/j.ijbiomac.2024.129377.

[63] S.B. Ahmed, H.I. Mohamed, A.M. Al-Subaie, A.I. Al-Ohali, N.M.R. Mahmoud, Investigation of the antimicrobial activity and hematological pattern of nano-chitosan and its nano-copper composite, Sci. Rep. 11 (2021) 9540, https://doi.org/10.1038/s41598-021-88907-z.

[64] S. Sathiyavimal, S. Vasantharaj, T. Kaliannan, H.A.L. Garalleh, M. Garaleh, K. Brindhadevi, N.T.L. Chi, A. Sharma, A. Pugazhendhi, Bio-functionalized copper oxide/chitosan nanocomposite using *Sida cordifolia* and their efficient properties of antibacterial, anticancer activity against on breast and lung cancer cell lines, Environ. Res. 218 (2023) 114986, https://doi.org/10.1016/j.envres.2022.114986.

[65] C. Gunawan, W.Y. Teoh, C.P. Marquis, R. Amal, Cytotoxic origin of copper(II) oxide nanoparticles: comparative studies with micron-sized particles, leachate, and metal salts, ACS Nano 5 (2011) 7214–7225, https://doi.org/10.1021/nn2020248.

[66] G. Applerot, J. Lellouche, A. Lipovsky, Y. Nitzan, R. Lubart, A. Gedanken, E. Banin, Understanding the antibacterial mechanism of CuO nanoparticles: revealing the route of induced oxidative stress, Small 8 (2012) 3326–3337, https://doi.org/10.1002/smll.201200772.

[67] O. Bondarenko, A. Ivask, A. Käkinen, A. Kahru, Sub-toxic effects of CuO nanoparticles on bacteria: kinetics, role of Cu ions and possible mechanisms of action, Environ. Pollut. 169 (2012) 81–89, https://doi.org/10.1016/j.envpol.2012.05.009.

[68] L. Macomber, C. Rensing, J.A. Imlay, Intracellular copper does not catalyze the formation of oxidative DNA damage in *Escherichia coli*, J. Bacteriol. 189 (2007) 1616–1626, https://doi.org/10.1128/JB.01357-06.

[69] J.D. Moore, A. Avellan, C.W. Noack, Y. Guo, G.V. Lowry, K.B. Gregory, Time-dependent bacterial transcriptional response to CuO nanoparticles differs from that of Cu^{2+} and provides insights into CuO nanoparticle toxicity mechanisms, Environ. Sci.: Nano 4 (2017) 2321–2335, https://doi.org/10.1039/C7EN00600D.

[70] Y. Li, W. Zhang, J. Niu, Y. Chen, Mechanism of photogenerated reactive oxygen species and correlation with the antibacterial properties of engineered metal-oxide nanoparticles, ACS Nano 6 (2012) 5164–5173, https://doi.org/10.1021/nn300934k.

[71] L. Macomber, J.A. Imlay, The iron-sulfur clusters of dehydratases are primary intracellular targets of copper toxicity, Proc. Natl. Acad. Sci. USA 106 (2009) 8344–8349, https://doi.org/10.1073/pnas.0812808106.

[72] D.K.C. Fung, W.Y. Lau, W.T. Chan, A. Yan, Copper efflux is induced during anaerobic amino acid limitation in Escherichia coli to protect iron-sulfur cluster enzymes and biogenesis, J. Bacteriol. 195 (2013) 4556–4568, https://doi.org/10.1128/JB.00543-13.
[73] G. Tan, Z. Cheng, Y. Pang, A.P. Landry, J. Li, J. Lu, H. Ding, Copper binding in IscA inhibits iron-sulphur cluster assembly in Escherichia coli, Mol. Microbiol. 93 (2014) 629–644, https://doi.org/10.1111/mmi.12676.
[74] G. Tan, J. Yang, T. Li, J. Zhao, S. Sun, X. Li, C. Lin, J. Li, H. Zhou, J. Lyu, H. Ding, Anaerobic copper toxicity and iron-sulfur cluster biogenesis in Escherichia coli, Appl. Environ. Microbiol. 83 (2017) e00867, https://doi.org/10.1128/AEM.00867-17, 17.
[75] A.D. Read, R.E.T. Bentley, S.L. Archer, K.J. Dunham-Snary, Mitochondrial iron–sulfur clusters: structure, function, and an emerging role in vascular biology, Redox Biol. 47 (2021) 102164, https://doi.org/10.1016/j.redox.2021.102164.
[76] M. Shi, H.S. Kwon, Z. Peng, A. Elder, H. Yang, Effects of surface chemistry on the generation of reactive oxygen species by copper nanoparticles, ACS Nano 6 (2012) 2157–2164, https://doi.org/10.1021/nn300445d.
[77] X. Chen, Z. Zhong, Z. Xu, L. Chen, Y. Wang, 2′,7′-Dichlorodihydrofluorescein as a fluorescent probe for reactive oxygen species measurement: forty years of application and controversy, Free Radic. Res. 44 (2010) 587–604, https://doi.org/10.3109/10715761003709802.
[78] J. Champer, J. Patel, N. Fernando, E. Salehi, V. Wong, J. Kim, Chitosan against cutaneous pathogens, Amb. Express 3 (2013) 1–8, https://doi.org/10.1186/2191-0855-3-37.
[79] B. Niu, G. Zhang, Effects of different nanoparticles on microbes, Microorganisms 11 (2023) 542, https://doi.org/10.3390/microorganisms11030542.